

## Using MSG-SEVIRI Cloud Physical Properties and Weather Radar Observations for the Detection of Cb/TCu Clouds

CINTIA CARBAJAL HENKEN\* AND MAURICE J. SCHMEITS

*Royal Netherlands Meteorological Institute (KNMI), De Bilt, Netherlands*

HARTWIG DENEKE

*Leibniz Institute for Tropospheric Research, Leipzig, Germany*

ROB A. ROEBELING

*Royal Netherlands Meteorological Institute (KNMI), De Bilt, Netherlands*

(Manuscript received 2 July 2010, in final form 11 February 2011)

### ABSTRACT

A new automated daytime cumulonimbus/towering cumulus (Cb/TCu) cloud detection method for the months of May–September is presented that combines information on cloud physical properties retrieved from the Spinning Enhanced Visible and Infrared Imager (SEVIRI) on board Meteosat Second Generation (MSG) satellites and weather radar reflectivity factors. First, a pixel-based convective cloud mask (CCM) is constructed on the basis of cloud physical properties [cloud-top temperature, cloud optical thickness (COT), effective radius, and cloud phase] derived from SEVIRI. Second, a logistic regression model is applied to determine the probability of Cb/TCu clouds for the collection of pixels that pass the CCM. In this model, MSG-SEVIRI cloud physical properties and weather radar reflectivity factors are used as potential predictor sources. The predictand is derived from aviation routine weather reports (METAR) made by human observers at Amsterdam Airport Schiphol for 2004–07. Results show that the CCM filters out >70% of the “no” events (no Cb/TCu cloud) and that >93% of the “yes” events (Cb/TCu cloud) are retained. Most skillful predictors are derived from radar reflectivity factors and the COT of high resolution. The derived probabilities from the combined MSG and radar method clearly show skill over sample climatology. Probability thresholds are used to convert derived probabilities into derived group memberships (i.e., yes/no Cb/TCu clouds). When comparing verification scores between the combined MSG and radar method and either the radar-only method or the MSG-only method, the combined MSG and radar method shows slightly better performance. When comparing the combined MSG and radar method with the current Royal Netherlands Meteorological Institute (KNMI) radar-based Cb/TCu cloud detection method, the two methods show comparable probability of detection, but the former shows a false-alarm ratio that is about 8% lower. Moreover, a big advantage of the newly developed method is that it provides probabilities, in contrast to the current KNMI method.

### 1. Introduction

Deep, convective clouds, such as towering cumulus (TCu) and cumulonimbus (Cb), play an important role in weather and climate through the transport of heat, moisture, and momentum from the earth's surface to the

free troposphere as well as through their impact on the earth's radiation budget. Observations of these clouds can be important source data for assimilation in weather forecasting and for monitoring climatological trends. Moreover, rapidly changing weather on different spatial and temporal scales may occur within and in the vicinity of these clouds and, therefore, have a serious impact on social–economic aspects of daily life.

The presence of associated severe weather can be relevant to, for example, the transport industry, tourism, the energy supply industry, the construction industry, and farmers. The Cb and TCu clouds may pose a serious risk to aviation through the hazardous weather, such as

---

\* Current affiliation: Institute for Space Sciences, Freie Universität Berlin, Berlin, Germany.

---

Corresponding author address: Dr. Rob A. Roebeling, EUMETSAT, Eumetsat Allee 1, D-64295 Darmstadt, Germany.  
E-mail: rob.roebeling@eumetsat.int

wind shear, heavy precipitation, and lightning, that is associated with these clouds. Also, aircraft in-flight icing may occur. Besides safety issues, hazardous weather increases annual costs in the aviation industry through the time and fuel losses that arise from delayed, canceled, and rerouted flights (Mecikalski et al. 2002).

Current techniques for detection and monitoring of convective clouds and convective precipitation and the nowcasting (i.e., forecasting of the weather within the next 6 h) of associated severe weather are mostly based on near-real-time information given by radar and satellite. In contrast to satellites, developing convective activity cannot be detected by radar until the precipitation stage has been reached. Also, radar networks are limited in their coverage, and spatial coverage can be reduced by ground shielding. Radars do provide information about vertical profiles within clouds, however, whereas satellite data mostly contain information about the upper part of the clouds or information integrated over the entire cloud profile.

In the 1970s and 1980s, much effort was made to estimate convective rainfall on the large scale, such as tropical rainfall, using infrared (IR) and visible (VIS) data from geostationary meteorological satellites. Infrared thresholds are identified that yield the best relationship between cloud-top brightness temperatures (BT) in satellite imagery and ground-based rainfall observations, mostly made by weather radars (e.g., Arkin 1979; Negri et al. 1984). VIS data are considered to be especially helpful in filtering out cirrus clouds. These clouds have cold cloud-top BTs but appear as transparent in the VIS images (King et al. 1995). Besides BTs, other multispectral techniques that use the difference between BTs in two spectral channels (BTD) can be helpful in identifying different cloud types (e.g., Inoue 1985; Kurino 1997; Schmetz et al. 1997; Tjemkes et al. 1997) and in deriving rainfall amounts (e.g., Amorati et al. 2000). Furthermore, BTs and BTDs have been used to identify cloud-top features and patterns significant to deep, convective clouds (e.g., Setvák and Doswell 1991; Levizzani and Setvák 1996).

Feature recognition and cloud classification can be done in an advanced manner using statistical classifiers whereby cloud pixels with similar spectral and textural properties within a satellite image are clustered, such as in neural networks (e.g., Bankert 1994) or fuzzy logic (e.g., Baum et al. 1997). Berendes et al. (2008) use an unsupervised clustering algorithm—standard deviation limited adaptive clustering—for convective cloud identification and classification in daytime satellite imagery. This clustering approach is the first step in the convective initiation product of the Advanced Satellite Aviation Weather Products (ASAP) initiative developed by the National Aeronautics and Space Administration (Mecikalski

et al. 2007). Tag et al. (2000) use a one-nearest-neighbor cloud classifier with spectral, textural, and physical features from VIS and IR images. In Donovan et al. (2006) this algorithm, which is developed by the Naval Research Laboratory, and two other algorithms, one from the National Center for Atmospheric Research (Herzogh et al. 2002) and one from the Aviation Weather Center (Mosher 2002), are intercompared. All three algorithms are based on geostationary satellite images and are used to identify convective cells that may present a hazard to aviation over the oceans.

By monitoring temporal trends in spectral bands, convective cloud development has been observed for quasi-stationary convection (Roberts and Rutledge 2003). Furthermore, cloud-tracking algorithms have been used to track and monitor temporal trends of individual convective cloud systems (e.g., Bolliger et al. 2003; Mecikalski and Bedka 2006; Zinner et al. 2008).

Multispectral techniques can be used to derive cloud physical properties for upper parts of the clouds. Cloud physical properties may include cloud-top temperature (CTT), cloud optical thickness (COT), particle size, liquid water path, and cloud phase (CPH). In turn, these cloud physical properties can be related to precipitation potential of clouds (e.g., Rosenfeld and Gutman 1994; Lensky and Rosenfeld 1997; Thies et al. 2008) or to the vigor of convective storms (Rosenfeld et al. 2008). The common principle of these multispectral techniques is that the cloud reflectances in the VIS wavelengths are primarily a function of COT while the cloud reflectances in the near-infrared (NIR) wavelengths are primarily a function of particle size (Nakajima and King 1990; Jolivet and Feijt 2003).

The ability to detect and monitor convective clouds in satellite images improves with increasing satellite resolution both in space and time. In January of 2004, the first Meteosat Second Generation (MSG) satellite of the new series of European geostationary satellites became operational. The onboard Spinning Enhanced Visible and Infrared Imager (SEVIRI) has an increased spatial resolution (3 km at nadir) and time resolution (15 min) relative to the resolutions of the first generations of Meteosat satellites. Also, the number of spectral channels (12) has increased, and a high-resolution (1 km at nadir) visible (HRV) channel is included. Therefore, it is expected that combining these relatively high resolution satellite data with weather radar observations will improve the detection of convective clouds with respect to current radar-based convective cloud detection methods.

In the Netherlands, Cb and TCu clouds are detected at regional airports using an adopted Météo-France radar algorithm (Leroy 2006) and data from a lightning detection network (Wauben et al. 2006). This Cb/TCu cloud detection method is part of the automated observation

system of present weather (AUTO METAR) at airports, which is operated by the Royal Netherlands Meteorological Institute (KNMI). The algorithm is based on radar reflectivity factor thresholds and area size of the precipitation echoes. It produces binary outcomes for the detection of Cb and TCu clouds.

In this paper we describe the derivation and verification of a new automated Cb/TCu cloud detection method for Amsterdam Airport Schiphol, which is the main airport of the Netherlands. In contrast to many other convective cloud detection methods, the focus in our detection method is not only on large-scale convective cloud systems but also on the detection of nonprecipitating clouds. The method combines weather radar observations with MSG-SEVIRI-derived cloud physical properties. The cloud physical properties are directly related to the presence of convective clouds in satellite images. They are related to convective clouds in a physical sense, by using a convective cloud mask (CCM), and in a statistical sense, by using logistic regression (Wilks 2006). This means that probabilities, which can be considered as a measure of uncertainty for the presence of Cb/TCu clouds, are produced for potential convective cloud areas indicated by the CCM. As a source for the predictand, which is the dependent variable to be derived (i.e., the presence or absence of Cb/TCu clouds), we have used aviation routine weather reports (METAR). These are weather reports made by human observers at airports. Potential predictors, which are the independent variables on which the prediction is based, have been derived from MSG-SEVIRI cloud physical properties as well as from weather radar observations. Special attention is given to a COT that has been derived at high resolution (1 km), which has not been used before in convective cloud detection methods.

The structure of this paper is as follows. In section 2 the METAR dataset and the dataset of the MSG-SEVIRI-derived cloud physical properties are described. Furthermore, the weather radar reflectivity factors are treated. In section 3 the Cb/TCu cloud detection method is presented. The predictand and predictor sources are described, as is the setup of this study, followed by the two steps involved in the detection method. The verification results of this method are treated in section 4. In section 5 a summary and the conclusions are given.

## 2. Datasets

### a. METAR

METAR is a format of a weather report about the current state of the weather at and in the vicinity of an airport. It is released on a routine basis and is mainly

used by pilots as part of the preflight preparations at other national and international airports. At Amsterdam Airport Schiphol, most meteorological information, such as wind speed and visibility, is measured automatically by instruments located at the airport. At all times, however, a human observer is present to monitor the weather. METARs are generated 2 times per hour, at 25 and 55 min past the hour. They include information about the weather over the last 10 min. The vicinity of an airport is defined as the area between approximately 8 and 16 km from the aerodrome reference point, which is the location of the human observer. Note that this area is estimated by the human observer.

A maximum of five cloud layers can be reported, with cloud cover and cloud-base height being reported for each layer. For Cb and TCu clouds only, cloud type is added to the report. The detection of these clouds is done visually by the human observer. One layer consisting of both Cb and TCu is reported as Cb cloud.

### b. MSG-SEVIRI cloud physical properties

The main instrument and payload on board MSG satellites is the optical radiometer SEVIRI, which observes the earth and its atmosphere in 12 spectral bands (Schmetz et al. 2002). At nadir view, the sampling distance for 11 channels is 3 km. For the HRV channel it is 1 km. The viewing area at the surface varies with the satellite viewing angle. This means that the spatial resolution of pixels in a satellite image decreases with increasing off-nadir viewing angle. The time resolution of the MSG imagery is 15 min.

At KNMI, SEVIRI data are utilized to retrieve cloud physical properties using the cloud physical properties (CPP) algorithm (Roebeling et al. 2006). These cloud physical properties include CTT, COT, effective radius (REFF), and CPH. The CPP algorithm retrieves these properties in two steps. First, satellite-observed VIS, NIR, and IR radiances are fed into a cloud detection scheme to create a cloud mask. Second, the Doubling-Adding KNMI (DAK) radiative transfer model (De Haan et al. 1987; Stammes 2001) is utilized to relate simulated VIS (0.6  $\mu\text{m}$ ) and NIR (1.6  $\mu\text{m}$ ) reflectances to observed 0.6- and 1.6- $\mu\text{m}$  reflectances for cloudy pixels. The DAK model is used to simulate cloud reflectances for predefined cloud physical properties and satellite viewing angles, which are stored in lookup tables (LUT). The COT and particle size are retrieved by comparing the simulated 0.6- and 1.6- $\mu\text{m}$  reflectances in the LUTs with the corresponding satellite reflectances.

The radiative effects of variations in the size of (water) cloud droplets are characterized through the REFF ( $\mu\text{m}$ ), which is defined as the ratio of the third moment and second moment of the particle size distribution (Hansen

and Hovenier 1974). For ice crystals, a volume equivalent REFF is assumed. The retrieval of COT and REFF is done in an iterative manner. The derived reflectances at the two wavelengths are repeatedly compared with the LUTs until both cloud physical properties converge to stable values.

From the 10.8- $\mu\text{m}$  BT and the emissivity of the cloud, the CTT can be derived. For optically thick clouds, the BT can be regarded as the thermodynamic temperature of the upper part of the cloud, in which the emissivity approaches a value of 1. For optically thin clouds, the observed BT also contains a significant contribution from the surface or underlying clouds. The BT is then corrected using the cloud (absorbing) optical thickness.

To discriminate between water and ice clouds (cloud thermodynamic phase), a consistency test of observed differences in cloud reflectance at 0.6 and 1.6  $\mu\text{m}$  is used, as well as a threshold test of the 10.8- $\mu\text{m}$  BT (CTT < 265 K). The differences in cloud reflectance at the two wavelengths arise from stronger absorption of radiation by ice particles than by water particles at the 1.6- $\mu\text{m}$  wavelength (Jolivet and Feijt 2003).

In addition to the cloud properties retrieved from MSG-SEVIRI at low resolution, an experimental COT product at HRV resolution is used in this study (HRV-COT). The increase (by a factor of 3) in spatial resolution allows for better resolution of the small-scale cloud variability. This HRV-COT product is based on the downscaling approach of Deneke and Roebeling (2010) for estimating the 0.6- $\mu\text{m}$  reflectance at HRV resolution. Low-frequency components of reflectance resolved by the 0.6- $\mu\text{m}$  channel are combined with high-frequency components measured by the HRV image—a procedure that relies on the substantial overlap of the spectral response functions and has been shown to be accurate to within a standard deviation of 0.01 in absolute reflectance. The values of CPH and REFF calculated at low resolution are then adopted for all  $3 \times 3$  enclosed high-resolution pixels, and the unique relation of 0.6- $\mu\text{m}$  reflectance and COT prescribed by the LUTs for constant REFF is inverted to obtain an estimate of COT for these  $3 \times 3$  pixel reflectances.

### c. Weather radar observations

Precipitation echoes, the intensities of which are measured in terms of radar reflectivity factors ( $\geq 7$  dBZ), are used to investigate the added value of using these weather radar observations, together with the MSG-SEVIRI-derived cloud physical properties, for the detection of convective clouds. In the Netherlands, two C-band Doppler weather radars are operated by KNMI. One weather radar is located at De Bilt (52.102°N, 5.178°E), and the second one is located at Den Helder (52.953°N, 4.790°E).

Precipitation and wind observations are made with a 14-elevation scan (between 0.3° and 25°), repeated every 5 min. From these scans, pseudo-constant altitude plan position indicator (CAPPI) images, which are horizontal cross sections of the radar reflectivity factor at a constant altitude, are made. The target height is 1500 m above antenna level. Until 2008, the horizontal resolution was  $2.4 \times 2.4 \text{ km}^2$ .

## 3. Method for the detection of Cb/TCu clouds

### a. Setup, predictand definition, and potential predictors

An automated Cb/TCu cloud detection method, which comprises two steps to be described in the following two sections, has been developed. Predictand and predictors have been derived from datasets for May–September of 2004–07. Because the cloud physical properties retrievals, both at low (3 km at nadir) and high (1 km at nadir) resolution, rely on VIS and NIR radiances, the Cb/TCu cloud detection method only considers daylight observations at solar zenith angles of  $< 70^\circ$ .

The Cb/TCu cloud reports in the METARs made at Amsterdam Airport Schiphol serve as a source for the predictand (i.e., the presence or absence of Cb/TCu clouds). Figure 1 shows climatological data for the Cb/TCu cloud reports in the METAR dataset for daytime hours between 0600 and 1800 UTC. First, we can clearly see the interannual, as well as the intraseasonal, variability of the Cb/TCu cloud reports. Second, Fig. 1 shows that the number of Cb cloud reports is much larger than the number of TCu cloud reports. This might be explained by the more pronounced characteristics of Cb clouds as compared with TCu clouds. The latter are often difficult to distinguish from Cu clouds, so that they will not be reported as often. In this study, we combined the Cb and TCu cloud reports to convert the METAR dataset into a binary dataset. Cases in which a Cb or TCu cloud has been reported in METAR are “yes events”; otherwise, they are “no events.” Because the distance at which the human observer will report Cb/TCu clouds in the METAR is subject to uncertainty, we trained and validated the Cb/TCu cloud detection method for circular observation areas with radii of 10, 20, and 30 km, as shown in Fig. 2. Amsterdam Airport Schiphol is located at the center of these circular observation areas.

The MSG-SEVIRI cloud physical properties and the weather radar observations serve as a pool of potential predictors.<sup>1</sup> The satellite viewing angle of MSG over the

<sup>1</sup> A previous version of the Cb/TCu cloud detection method was also tested with lightning data, but it did not show an improvement (Carbajal Henken et al. 2009).

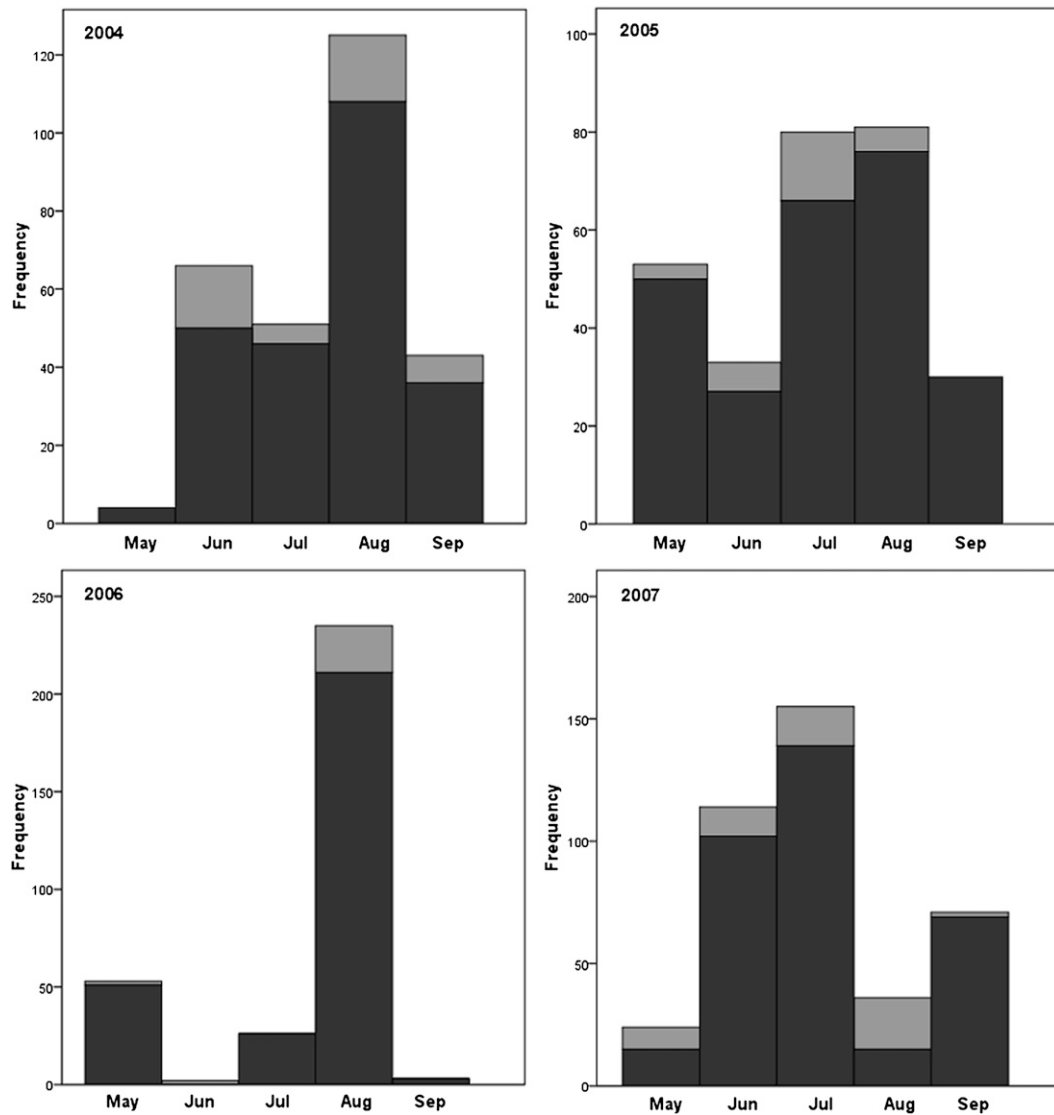


FIG. 1. Daytime METAR Cb/TCu cloud climatological data for May–September of 2004–07. The gray bars indicate the number of TCu cloud reports. The black bars indicate the number of Cb cloud reports.

Netherlands is about 60°. This results in pixel dimensions of about 4 × 7 km<sup>2</sup> for the spatial low-resolution data and about 1 × 2 km<sup>2</sup> for the spatial high-resolution data. Both the low-resolution cloud physical properties and the weather radar observations are interpolated to the high resolution of the HRV observations. By doing so, all predictors are available at the high resolution of the VIS channel.

The two METAR time steps each hour are matched to the four MSG time steps each hour by relating each METAR time step (25 or 55 min past the hour) to two MSG time steps (11 and 26 or 41 and 56 min past the hour). The four MSG time steps do not fall within the 10-min reporting time of the two METAR reports.

The difference between the METAR time period and the two corresponding MSG time steps, however, is only 1 and 4 min, respectively. It is assumed that within those 1- and 4-min periods the cloud fields within the circular observation area will only change slightly.

The MSG-SEVIRI cloud physical properties are corrected for parallax shifts, which are largest for high clouds at higher latitudes. Hourly temperature profiles from the European Centre for Medium-Range Weather Forecasts model for Cabauw, Netherlands (51.971°N, 4.927°E), are used to relate MSG-SEVIRI CTT to cloud-top height. The amount of parallax shift toward the north is calculated for the highest cloud tops, which are assumed to be represented by the 2.5% of coldest cloud tops with COTs



FIG. 2. Moderate Resolution Imaging Spectroradiometer (MODIS) satellite image of the Netherlands, 6 May 2000. The three circular observation areas with radii of 10, 20, and 30 km are shown. The plus sign at the center of the circles indicates the location of Amsterdam Airport Schiphol.

of  $>50$ . In this study, a cloud height of about 10 km at a latitude of  $52^\circ$  results in a parallax shift of about 16 km toward the north.

To train and validate the Cb/TCu cloud detection method, the potential predictors and predictand datasets are divided into a training dataset ( $\sim 70\%$ ) and a validation ( $\sim 30\%$ ) dataset. This is done by randomly selecting about 70% of all days using a Bernoulli distributed random variate with a 0.7 probability parameter. By doing this random selection on days and assuming that Cb/TCu cloud reports made on different days do not represent the same event, an independent validation dataset is obtained.

For several time steps the MSG-SEVIRI data are missing as a result of problems with the data reception system. These time steps are not considered in the training and validation datasets. In addition, the time steps at which the solar zenith angle is  $>70^\circ$  were also excluded, since the retrieval of cloud physical properties becomes very uncertain at large solar zenith angles.

TABLE 1. Investigated thresholds of the cloud physical properties, i.e., HRV-COT and HRV-COT standard deviation, CTT (K), and  $\text{REFF}_{\text{water}}$  ( $\mu\text{m}$ ) for the development of the CCM.

| Cloud physical properties    | Investigated thresholds   |
|------------------------------|---|
| HRV-COT                      | $>6, 8, 10, 15, 20, 30, 40, 50$                                     |
| CTT                          | $<285, 280, 279, 278, 277, 276, 275, 274, 273, 270, 265, 260$       |
| $\text{REFF}_{\text{water}}$ | $>8, 10, 12, 13, 14, 16, 18$  |
| HRV-COT std dev (HRV-COT)    | $>4, 5, 6, 8, 10, 15, 20, 30, 50$<br>(if $<50, 60, 100, 150, 200$ ) |

### b. Convective cloud mask

The first step in the Cb/TCu cloud detection method is the CCM. The principle of the CCM is to use cloud physical properties to identify convective clouds in a satellite image. Well-developed convective clouds, such as Cb and TCu clouds, show large vertical growth. These clouds exhibit low CTTs and high COTs. In the usual case, relatively large water droplets or ice crystals are present in the upper parts of these clouds. Moreover, convective clouds often exhibit a lumpy texture, which is caused by shadow effects of the irregularly shaped cloud tops. A group of organized convective cells can also contribute to an increase in the spatial variability in satellite images.

Using a threshold technique, the CCM determines for each pixel within a satellite image whether it might represent a convective cloud. This pixel-based mask is made for the circular observation areas at each time step. Table 1 shows the investigated threshold combinations for the CCM. A pixel has to meet all of the criteria to pass the CCM. The collection of pixels passing the CCM at each time step is considered to represent convective clouds. Pixels that do not pass the CCM are not considered in further calculations.

To determine the optimum combination of cloud physical properties thresholds for a CCM retrieval that retains at least 95% of the yes events and removes a large part of the no events, the training dataset was used to examine the CCM for the threshold combinations listed in Table 1. This examination was done for circular observation areas with radii of 10, 20, and 30 km (see Fig. 2). Although human observers are instructed to report Cb/TCu clouds at and in the vicinity of the airport, the definition of vicinity is very likely to be stretched (e.g., in the case of well-developed Cb clouds, which can be visible at large distances). The results show that none of the threshold combinations yielded the specified criterion for the circular observation areas with radii of 10 and 20 km. The requirement that at least 10 high-resolution pixels within the observation area should be flagged as convective clouds prevents more than 95% of the yes events from passing the CCM. Therefore, we decided

TABLE 2. Best threshold combination of the cloud physical properties, i.e., HRV-COT and HRV-COT standard deviation, CTT (K), and REFF<sub>water</sub> (μm) in the CCM for the training dataset.

| HRV-COT | CTT    | REFF <sub>water</sub> | HRV-COT<br>std dev | (HRV-COT) |
|---------|--------|-----------------------|--------------------|-----------|
| >8      | <275 K | >12 μm                | >5                 | (if <100) |

to continue the development of an automated Cb/TCu cloud detection method using a CCM for a circular observation area with a radius of 30 km only.

The “best” threshold combination yielded with the training dataset is shown in Table 2. Then, over 95% of the yes events remain while over 70% of the no events are removed. The HRV-COT threshold of 8 is well within the range of transition values from optically thin to optically thick clouds often used in cloud studies. In addition, the particle size retrievals are most accurate for these optically thick clouds, for which the 1.6-μm reflectance is mainly a function of particle size (Nakajima and King 1990; Roebeling et al. 2006). The REFF threshold of 12 μm for water droplets is close to 14 μm, which can be considered to be the threshold at which water droplets in optically thick clouds have grown large enough to initiate the precipitation process that can be detected by weather radars (Rosenfeld and Gutman 1994), suggesting that the cloud has reached its mature stage. Remember that particles assigned to the ice phase do not need to meet the REFF threshold in the CCM. The CTT threshold of 275 K is close to the freezing level, which is located between 2- and 5-km height during the summer half year. Furthermore, we used the standard deviation on high-resolution COT (HRV-COT standard deviation) to find spatial variability within a satellite image. This is similar to Mecikalski et al. (2010), who use texture in HRV data to discern aspects of cumulus clouds. The standard deviation is calculated for the center pixel of a 3 × 3 pixel-size box. This threshold is not set very strictly and only holds for center pixels with HRV-COT values of less than 100, but HRV-COT standard deviation still shows a contribution to the reduction of the number of no events.

*c. Logistic regression model*

The second step in the Cb/TCu cloud detection method is a logistic regression model (Wilks 2006). Logistic regression models are used in situations in which one wants to predict the probability of the occurrence of an event based on values of a set of predictors. The variable of interest, or predictand, is binary. The predictor variables can be of any type. In meteorological research, logistic regression has been applied to, for example, short-term forecasting of thunderstorms (Schmeits et al. 2008),

TABLE 3. Potential predictors derived from the MSG-SEVIRI cloud physical properties for the collection of pixels flagged as convective cloud pixels in the CCM and from the weather radar observations for all pixels in the circular observation area.

| Cloud physical properties            | Radar                                |
|--------------------------------------|--------------------------------------|
| Mean                                 | Mean                                 |
| Median                               | Median                               |
| Std dev                              | Std dev                              |
| Min (2.5th percentile)               | Min (2.5th percentile)               |
| Max (97.5th percentile)              | Max (97.5th percentile)              |
| Range (2.5th–97.5th percentiles)     | Range (2.5th–97.5th percentiles)     |
| Percentiles (17th, 25th, 75th, 83rd) | Percentiles (17th, 25th, 75th, 83rd) |
|                                      | No. of pixels >30 dBZ                |
|                                      | No. of pixels >40 dBZ                |

short-term forecasting of premonsoon convective developments (Dasgupta and De 2007), and forecasting of large hail Billet et al. (1997). Furthermore, it has been used as a tool to investigate the difference between the present weather reported by a human observer and present weather reports produced by automated weather stations (Merenti-Välimäki and Laininen 2002).

Logistic regressions are fit to a binary predictand using the nonlinear equation (Wilks 2006)

$$P(y) = \frac{1}{1 + \exp[-(a_0 + a_1x_1 + a_2x_2 + \dots + a_nx_n)]}, \tag{1}$$

where  $P(y)$  is the probability that an event  $y$  occurs,  $x_i$  ( $i = 1, 2, \dots, n$ ) is the set of predictors, and  $a_i$  ( $i = 1, 2, \dots, n$ ) are the regression coefficients. Predictors are selected using a forward stepwise selection method. At each step, a predictor is entered or removed from the model based on a significance threshold. The predictor that results in the best regression when combined with previously selected predictors while also meeting the significance criterion enters the model. The regression coefficients are determined using a maximum likelihood method (Wilks 2006). It is an iterative method, which maximizes the product of all computed probabilities of the (non-) occurrence of the event in the training dataset.

The MSG-SEVIRI-derived cloud physical properties and weather radar observations are used as potential predictor sources. To create a number of potential predictors from the MSG-SEVIRI cloud physical properties, we have calculated several statistics for pixels flagged as convective clouds in the first step of the detection method (Table 3). To create a number of potential predictors from the radar reflectivity factors, we have calculated several statistics for all pixels in the circular observation area, also shown in Table 3. At each time step one probability is determined for the circular

observation area. This probability provides a measure of uncertainty about the actual presence of Cb/TCu clouds within the surroundings of the airport. The collection of pixels passing the CCM indicates the areas of potential deep, convective clouds. A minimum number of 10 high-resolution pixels passing the CCM is used to assure proper statistical calculations.

We decided to include in the model only the most frequently selected predictor associated with each cloud physical property used in the CCM, with the exception of HRV-COT. Despite the fact that more predictors from the same cloud physical property might have a significant contribution to the model, they are often correlated, and limiting the number of predictors also minimizes the problem of overfitting.

Applying forward stepwise selection to the training dataset shows that the predictors' radar reflectivity factor maximum (RR max), HRV-COT standard deviation maximum, HRV-COT minimum, REFF median, and CTT maximum form a well-performing set of predictors. The RR max is identified as the most skillful predictor, followed by the predictors derived from the HRV-COT. All but the HRV-COT minimum show a positive regression coefficient. This means that the probability of the presence of Cb/TCu clouds increases with increasing RR max, HRV-COT standard deviation maximum, REFF median, and CTT maximum and decreases with increasing HRV-COT minimum.

The forward stepwise selection method did not show any significant difference in the set of selected predictors for different periods during the day (morning, 0600–1000 UTC; midday, 1000–1400 UTC; afternoon, 1400–1800 UTC) or during the year (spring; early summer; late summer).

Because of the different time resolutions of the MSG-SEVIRI observations and the METAR observations, two MSG time steps are related to one METAR time step, and therefore two probabilities are calculated for each METAR time step. When using the highest of the two probabilities for training against METAR, the highest Brier skill score (BSS; Wilks 2006) is achieved for the training dataset when compared with using the lowest probability or the mean of the two probabilities. Therefore, for verification of the detection method with the validation dataset the higher of the two probabilities is used when comparing with each METAR time step.

#### 4. Verification results

##### a. Convective cloud mask

For verification of the CCM we applied the optimal threshold combination that was derived from the training dataset to the validation dataset. For the validation dataset,

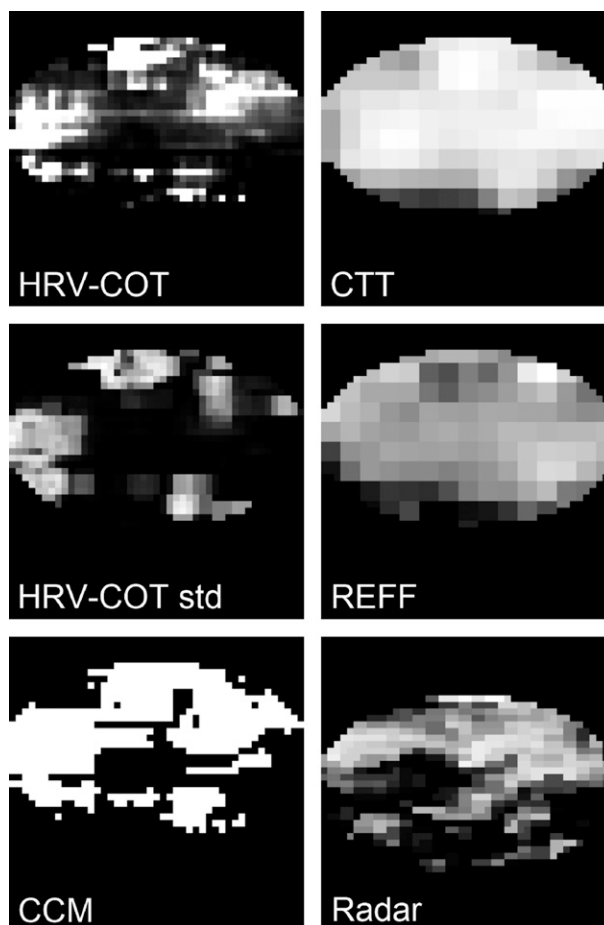


FIG. 3. (bottom left) An example of the CCM at 1426 UTC 30 Aug 2004. This day is part of the validation dataset. From top to bottom and from left to right the panels show HRV-COT (range 8–50), CTT (range 200–275 K), HRV-COT standard deviation (range 5–150), REFF (range 12–56  $\mu\text{m}$ ), resulting CCM, and radar (range 0–50 dBZ). Brighter pixels indicate higher values, except for CTT values, which are inverted.

93% of the yes events remain while again over 70% of the no events are removed. This results in a probability of detection (POD) and false-alarm ratio (FAR) (Wilks 2006) of 93% and 69%, respectively, with a frequency of occurrence of the yes events of 12%. Figure 3 shows an example of pixel values for HRV-COT, CTT, HRV-COT standard deviation, and REFF (top four panels) for pixels within the circular observation area. The bottom two panels in Fig. 3 show the resulting CCM and a radar image for comparison. In this example, the pattern of the collection of pixels passing the CCM is mostly related to the pattern of high HRV-COT values, which is, however, not always the case.

##### b. Probabilities

To verify the probabilities derived from the Cb/TCu cloud detection method for the validation dataset, an

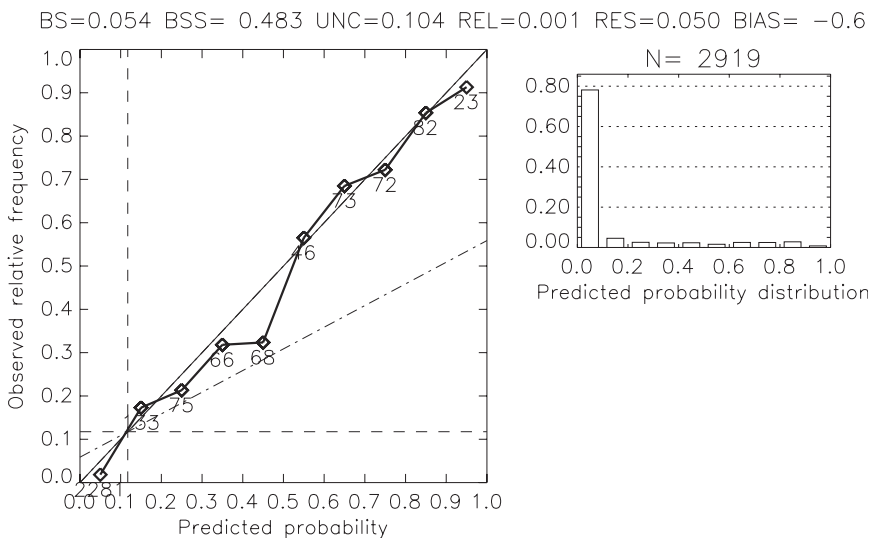


FIG. 4. Attributes diagram for the combined MSG and radar detection method, for the validation dataset. The observed frequencies of Cb/TCu cloud occurrence are shown (diamonds), conditional on each of the 10 possible derived probabilities. For a perfectly reliable detection method, these points would be located on the perfect-reliability line (diagonal). The dashed lines indicate the sample climatology. The dash-dotted line indicates the no-skill line. The histogram on the right shows the relative frequency of the derived probabilities. Here,  $N$  is the total number of events, BS is Brier score, BSS is Brier skill score, UNC is uncertainty, REL is reliability, and RES is resolution (Wilks 2006).

attributes diagram (Wilks 2006), shown in Fig. 4, is used. The derived probabilities have been divided into 10% bins. For a reliable detection method, the derived probabilities in a 10% bin have to be close to the observed relative frequency of this 10% bin. In the case of a perfectly reliable detection method, the points are located on the perfect-reliability (1:1) line. The no-resolution line in the attributes diagram, which is equal to the horizontal dashed line that also indicates the sample climatology, relates to the resolution term in the Brier score (BS) decomposition (Wilks 2006). Above the panels in Fig. 4, the BS, its three components (reliability, resolution, and uncertainty), and the BSS are presented. We used the sample climatology as a reference to compute the BSS. The attributes diagram clearly indicates skill due to good resolution and reliability; the latter can be seen because the points are located close to the perfect-reliability line. The Cb/TCu cloud detection method shows slight underwarning (negative bias). Furthermore, we see that all points are located closer to the perfect-reliability line than to the no-resolution line, which means that they contribute positively to detection skill.

To investigate the skill of the detection methods for different Cb/TCu cloud climatologies during the summer daytime period, we performed bootstrapping on the derived probabilities in the validation dataset using 10 000 samples. With a confidence interval of 95%, values

of the BSS range between 0.431 and 0.532 for the combined MSG and radar detection method. The BSS value is clearly positive, indicating skill over the sample climatology.

*c. Probability threshold*

We used probability thresholds to convert the derived probabilities into a binary predictand, that is, the presence or absence of Cb/TCu clouds within the circular observation area at a given time step. Cases with derived probabilities that are below the probability threshold are labeled as no events, and cases with derived probabilities that are equal to or greater than the probability threshold are labeled as yes events. By producing binary outcomes, the performance of the logistic regression models can be compared directly with the current KNMI radar-based Cb/TCu cloud detection method (Wauben et al. 2006). Note that information is lost on the uncertainty of the occurrence of the event when converting derived probabilities into a binary predictand.

Figure 5 presents the POD, FAR, accuracy (ACC), and critical success index (CSI) (Wilks 2006) for probability thresholds between 5% and 95% with steps of 5% for the combined MSG and radar detection method. These verification scores were calculated from contingency tables (Wilks 2006) that were composed for all thresholds. Figure 5 shows that the POD and FAR

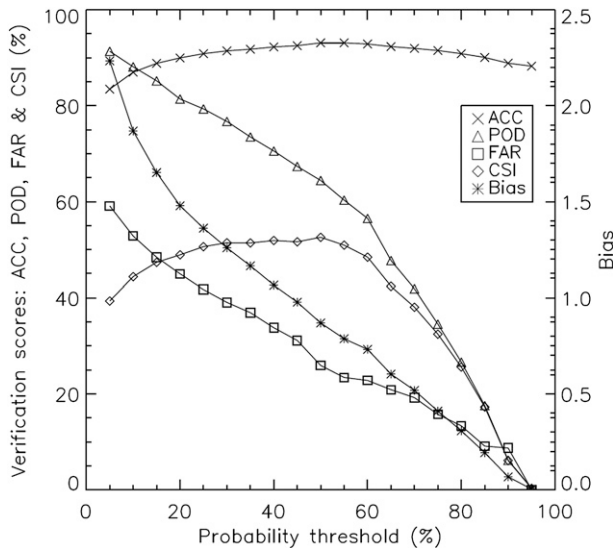


FIG. 5. Verification scores for the validation dataset as a function of the probability threshold (in steps of 5%) for the combined MSG and radar detection method. The score acronyms are defined in the text.

decrease for increasing probability thresholds. The ACC reaches maximum values at probability thresholds around 45%–55% but only shows slight variations. The CSI has a maximum value of 53% at a probability threshold of 50% but only shows minor variations for probability thresholds between 30% and 55%. The choice of a best probability threshold depends on user preferences and/or the user's cost–loss ratio (Katz and Murphy 2005).

Figure 6 shows the CSI and bias as functions of POD and FAR for six probability thresholds between 30% and 55%. The best verification scores are located in the top-left corner of Fig. 6 near the diagonal (bias = 1) line. The label  $\times_{30}$  in the figure indicates the verification scores of the KNMI radar-based Cb/TCu cloud detection method, which is also for a circular observation area with a radius of 30 km.

In addition, we compared the combined MSG and radar detection method with the results of logistic regression models, including predictors derived from radar reflectivity factors only (radar only), and predictors derived from MSG-SEVIRI cloud physical properties only (MSG only). Note that for the radar-only detection method no CCM is used, whereas it *was* used for the MSG-only detection method (also with a radius of 30 km). The number of predictors included in the radar-only and MSG-only detection methods is equal to the number of predictors included in the combined MSG and radar detection method, which is equal to five predictors. For the radar-only detection method, forward

stepwise selection shows again that RR max is the most skillful predictor. Apart from RR max, the radar reflectivity factor 83rd percentile, the number of pixels with radar reflectivity factors >30 dBZ, the radar reflectivity factor median, and the radar reflectivity factor minimum are also included in the radar-only detection method. For the MSG-only detection method, forward stepwise selection shows that the HRV–COT range is the most skillful predictor. Furthermore, the HRV–COT standard deviation maximum, REFF median, CTT range, and CTT standard deviation are included in the MSG-only logistic regression model.

In Fig. 6, it is shown that the radar-only detection method shows slightly better performance than the MSG-only detection method for probability thresholds that result in a bias nearest to 1. In turn, the combined MSG and radar detection method shows a slight improvement in performance when compared with the radar-only detection method. More details on the comparison of different logistic regression models can be found in Carbajal Henken et al. (2009).

## 5. Summary and conclusions

This paper presents a novel automated Cb/TCu cloud detection method for daytime hours. The method has been developed for the months of May–September of 2004–07 using METAR Cb/TCu cloud observations at Amsterdam Airport Schiphol in the Netherlands. The Cb/TCu cloud detection method is carried out in two steps. First, a CCM is created from MSG-SEVIRI cloud physical properties (HRV–COT, CTT, REFF, and HRV–COT standard deviation), which provides spatial information about the presence of convective clouds. Second, a logistic regression model is used to determine the probability that the cloudy pixels in the CCM represent Cb/TCu clouds. As a predictand source, we used the Cb/TCu cloud observations from METAR made at Amsterdam Airport Schiphol, and the set of potential predictors has been derived from MSG-SEVIRI cloud physical properties and weather radar reflectivity factors. The combined use of these predictors has the advantage that both precipitating and nonprecipitating Cb/TCu clouds can be detected. Our method is novel in the sense that satellite-retrieved cloud physical properties are directly related to the presence of convective clouds in satellite images. Besides the use of cloud physical property retrievals from the low-resolution channels of MSG-SEVIRI, our method also uses the newly developed COT retrievals from the HRV channel of MSG-SEVIRI. The advantage of this high-resolution COT instead of reflectances lies in the fact that reflectances not only depend on the physical properties of the

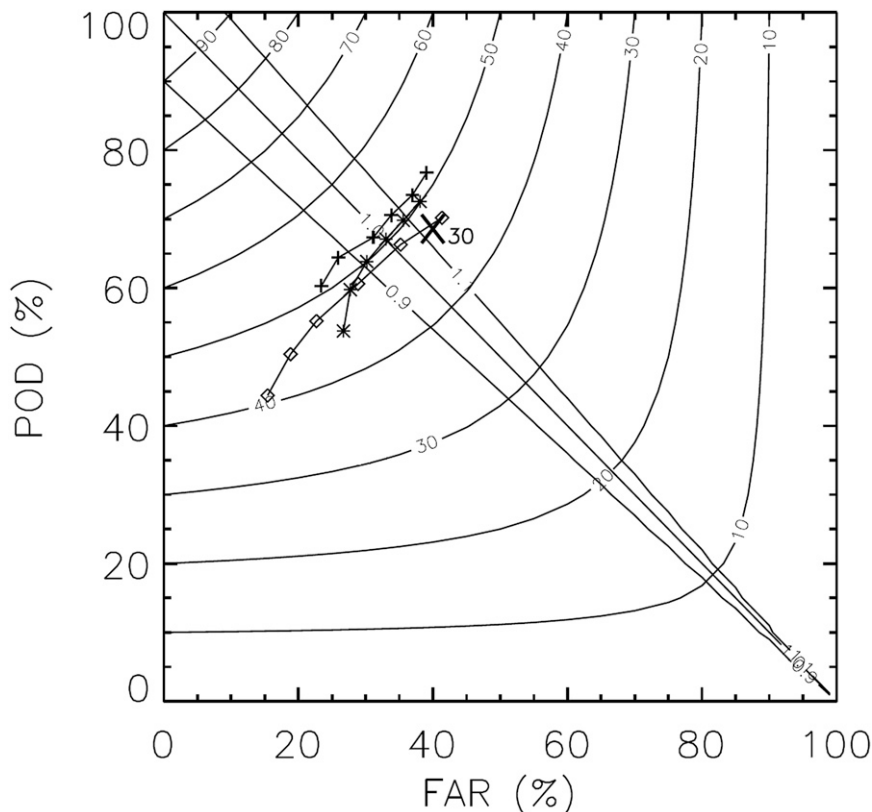


FIG. 6. CSI (bent contour lines) and bias (straight contour lines) as functions of POD and FAR. The four verification scores are shown for six probability thresholds (from 30% to 55%, thresholds increase from top-right points to bottom-left points for a given line) for the combined MSG and radar detection method (plus signs), radar-only detection method (asterisks), and MSG-only detection method (diamonds). The  $\times_{30}$  label shows the scores of the current KNMI radar-based Cb/TCu cloud detection method for a circular observation area with a radius of 30 km.

clouds but also depend on, for example, viewing geometry, whereas for derived cloud physical properties these effects are taken into account.

When using a circular observation area of 30 km, the CCM filters out about 70% of the no events while 93% of the yes events are retained in the validation dataset. This results in a POD and FAR of 93% and 69%, respectively, with a frequency of occurrence of the yes event of 12%. In the combined MSG and radar logistic regression model, the most important predictor is derived from radar reflectivity factors, followed by two predictors derived from the high-resolution COT (HRV-COT and HRV-COT standard deviation). In addition, two predictors derived from the REFF and CTT are added to the set of predictors. Note that similar cloud physical properties are used in the CCM and in the logistic regression model. The prominence of the HRV-COT demonstrates the additional information content of the improved spatial resolution offered by the HRV

channel for Cb/TCu cloud detection. The highly positive BSS for the validation dataset clearly shows skill over the sample climatology. For a probability threshold with minimal bias and maximal CSI value, the POD and FAR values of the combined MSG and radar logistic regression model are 67% and 31%, respectively. The selected MSG-SEVIRI predictors suggest that the standard resolution of the SEVIRI instrument of  $3 \times 3 \text{ km}^2$  at nadir is insufficient to resolve fully the formation and development of convective clouds. Consistent with our findings, Zinner et al. (2008) relied upon the HRV channel for tracking of convective cells, and Deneke et al. (2009) reported that reflectances observed at the SEVIRI standard resolution were not sufficient to resolve fully the cloud-induced variability in surface measurements.

In logistic regression models, it is very likely that several subsets of predictors have near-equal performance because of correlations among these predictors. Therefore, we compared the results of the combined MSG and

radar logistic regression model with those obtained with a radar-only and an MSG-only logistic regression model. In comparing the results of these models, the added value of combining MSG-SEVIRI cloud physical properties and weather radar reflectivity factors for the detection of Cb/TCu clouds could be assessed. Although the most skillful predictors selected by the logistic regression model differ among these three models—that is, the maximum value of the radar reflectivity factors (97.5th percentile) for the combined MSG and radar and radar-only logistic regression models and the HRV-COT range for the MSG-only logistic regression model—their verification scores are similar. The combined MSG and radar detection method performs only slightly better than the MSG-only and radar-only detection method (Fig. 6). Because METAR reports, which have been used as the predictand source for the Cb/TCu cloud observations, are subjective, the above-summarized results should be interpreted with care. There are two reasons why the METAR reports are subjective. First, no exact rules exist for determining the transition of a cumulus cloud into a towering cumulus. Second, the maximum viewing/reporting range of the observer is not determined exactly. Thus, it is very likely that deep, convective clouds at large distances are still being reported. This cannot be verified with METAR, because no information on the position of the reported clouds is included.

The qualitative advantage of the MSG-only detection method over the radar-only detection method lies in the quasi-global coverage of the MSG satellite, which is by far superior to the coverage of radar networks, and in the detection of nonprecipitating convective clouds. The latter is unfortunately difficult to verify because of the lack of accurate and statistically sufficient observations of TCu clouds. Our study showed that the use of logistic regression helps to improve the detection of Cb/TCu clouds. This is shown by the comparison of the radar-only detection method with the current KNMI radar-based detection method. Both methods have similar POD values, but the FAR of the radar-only detection method is about 8% lower than the FAR of the KNMI detection method. Another large advantage of the newly developed method is that it provides probabilities, in contrast to the radar-based KNMI detection method and many other convective cloud detection methods.

Our method differs from other convective cloud detection methods in the sense that it detects both small- and large-scale, precipitating and nonprecipitating, convective cloud systems within a limited observing area, whereas other methods concentrate rather on the detection of large-scale convective cloud systems observed over much wider areas (e.g., Mosher 2002). Moreover, most convective cloud detection methods are verified

against collocated radar observations (e.g., Mecikalski et al. 2008), which implies that their focus is on the detection of precipitating convective cloud systems and/or lightning (e.g., Zinner et al. 2008). These differences, and the fact that the verification periods and areas differ, make a direct quantitative comparison of our detection method with other detection methods impossible.

At KNMI, similar Cb/TCu cloud detection methods are presently being developed for the nighttime period and the wintertime period, and for regional airports as well. Future improvements may be achieved by using other cloud physical properties retrieved at high resolution, taking advantage of the spatial variability as present in the HRV channel of SEVIRI. Further improvements may also be expected from potential predictors that are derived from temporal trends in cloud physical properties using an advanced cloud-tracking algorithm. The research done by Mecikalski and Bedka (2006) and Zinner et al. (2008) forms a baseline for these developments. Also, a new set of potential predictors can be derived from numerical weather prediction model data and from sounding observations.

*Acknowledgments.* The authors thank Kees Kok (KNMI) for his advice on verification scores and his suggestion to include Fig. 6, Iwan Holleman (formerly at KNMI) for providing weather radar observations, Joost Postma (KNMI) for his information on METARs at the Amsterdam Airport Schiphol weather station, Rudolf van Westrhenen (KNMI) for running the present KNMI radar-based algorithm for validation, and Erwin Wolters (KNMI) and Paul de Valk (KNMI) for their comments on an earlier version of this manuscript. Comments from the two anonymous reviewers are acknowledged and helped to improve the manuscript.

## REFERENCES

- Amorati, R., P. Alberoni, V. Levizzani, and S. Nanni, 2000: IR-based satellite and radar rainfall estimates of convective storms over northern Italy. *Meteor. Appl.*, **7**, 1–18.
- Arkin, P., 1979: The relationship between fractional coverage of high cloud and rainfall accumulations during GATE over the B-scale array. *Mon. Wea. Rev.*, **107**, 1382–1387.
- Bankert, R., 1994: Cloud classification of AVHRR imagery in maritime regions using a probabilistic neural network. *J. Appl. Meteor.*, **33**, 909–918.
- Baum, B., V. Tovinkere, J. Titlow, and R. Welch, 1997: Automated cloud classification of global AVHRR data using a fuzzy logic approach. *J. Appl. Meteor.*, **36**, 1519–1540.
- Berendes, T., J. Mecikalski, W. MacKenzie Jr., K. Bedka, and U. Nair, 2008: Convective cloud identification and classification in daytime satellite imagery using standard deviation limited adaptive clustering. *J. Geophys. Res.*, **113**, D20207, doi:10.1029/2008JD010287.

- Billet, J., M. DeLisi, B. Smith, and C. Gates, 1997: Use of regression techniques to predict hail size and the probability of large hail. *Wea. Forecasting*, **12**, 154–164.
- Bolliger, M., P. Binder, and A. Rossa, 2003: Tracking cloud patterns by Meteosat rapid scan imagery in complex terrain. *Meteor. Z.*, **12**, 73–80.
- Carbajal Henken, C. K., M. J. Schmeits, E. L. A. Wolters, and R. A. Roebeling, 2009: Detection of Cb and TCu clouds using MSG-SEVIRI cloud physical properties and weather radar observations. KNMI WR 2009-04, 97 pp. [Available online at <http://www.knmi.nl/publications/showAbstract.php?id=7203>.]
- Dasgupta, S., and U. De, 2007: Binary logistic regression models for short term prediction of premonsoon convective developments over Kolkata (India). *Int. J. Climatol.*, **27**, 831.
- De Haan, J., P. Bosma, and J. Hovenier, 1987: The adding method for multiple scattering calculations of polarized light. *Astron. Astrophys.*, **183**, 371–391.
- Deneke, H., and R. Roebeling, 2010: Downscaling of Meteosat SEVIRI 0.6 and 0.8 micron channel radiances utilizing the high-resolution visible channel. *Atmos. Chem. Phys. Discuss.*, **10**, 10 707–10 740.
- , W. Knap, and C. Simmer, 2009: Multiresolution analysis of the temporal variance and correlation of transmittance and reflectance of an atmospheric column. *J. Geophys. Res.*, **114**, D17206, doi:10.1029/2008JD011680.
- Donovan, M., E. Williams, C. Kessinger, G. Blackburn, P. Herzegh, R. Bankert, S. Miller, and F. Mosher, 2006: The identification and verification of hazardous convective cells over oceans using visible and infrared satellite observations. Preprints, *12th Conf. on Aviation Range and Aerospace Meteorology*, Atlanta, GA, Amer. Meteor. Soc., P1.20. [Available online at <http://ams.confex.com/ams/pdfpapers/103764.pdf>.]
- Hansen, J., and J. Hovenier, 1974: Interpretation of the polarization of Venus. *J. Atmos. Sci.*, **31**, 1137–1160.
- Herzegh, P., E. Williams, T. Lindholm, F. Mosher, C. Kessinger, R. Sharman, J. Hawkins, and D. Johnson, 2002: Development of automated aviation weather products for oceanic/remote regions: Scientific and practical challenges, research strategies, and first steps. Preprints, *10th Conf. on Aviation, Range, and Aerospace Meteorology*, Portland, OR, Amer. Meteor. Soc., 57–60.
- Inoue, T., 1985: On the temperature and effective emissivity determination of semi-transparent cirrus clouds by bi-spectral measurements in the 10  $\mu\text{m}$  window region. *J. Meteor. Soc. Japan*, **63**, 88–99.
- Jolivet, D., and A. Feijt, 2003: Cloud thermodynamic phase and particle size estimation using the 0.67 and 1.6  $\mu\text{m}$  channels from meteorological satellites. *Atmos. Chem. Phys. Discuss.*, **3**, 4461–4488.
- Katz, R., and A. Murphy, 2005: *Economic Value of Weather and Climate Forecasts*. Cambridge University Press, 240 pp.
- King, P., W. Hogg, and P. Arkin, 1995: The role of visible data in improving satellite rain-rate estimates. *J. Appl. Meteor.*, **34**, 1608–1621.
- Kurino, T., 1997: A satellite infrared technique for estimating deep/shallow precipitation. *Adv. Space Res.*, **19**, 511–514.
- Lensky, I., and D. Rosenfeld, 1997: Estimation of precipitation area and rain intensity based on the microphysical properties retrieved from NOAA AVHRR data. *J. Appl. Meteor.*, **36**, 234–242.
- Leroy, M., 2006: Status of the automatic observation on aerodrome and ongoing improvements in France. *Proc. TECO-2006—WMO Tech. Conf. on Meteorological and Environmental Instruments and Methods of Observation*, Geneva, Switzerland, World Meteorological Organization, 8 pp. [Available online at [http://www.wmo.int/pages/prog/www/IMOP/publications/IOM-94-TECO2006/1\(3\)\\_Leroy\\_France.pdf](http://www.wmo.int/pages/prog/www/IMOP/publications/IOM-94-TECO2006/1(3)_Leroy_France.pdf).]
- Levizzani, V., and M. Setvák, 1996: Multispectral, high-resolution satellite observations of plumes on top of convective storms. *J. Atmos. Sci.*, **53**, 361–369.
- Mecikalski, J., and K. Bedka, 2006: Forecasting convective initiation by monitoring the evolution of moving cumulus in daytime GOES imagery. *Mon. Wea. Rev.*, **134**, 49–78.
- , and Coauthors, 2002: NASA Advanced Satellite Aviation-Weather Products (ASAP) study report. NASA Tech. Rep., 65 pp. [Available from Schwerdtfeger Library, 1225 West Dayton St., University of Wisconsin—Madison, Madison, WI 53706.]
- , and Coauthors, 2007: Aviation applications for satellite-based observations of cloud properties, convection initiation, in-flight icing, turbulence, and volcanic ash. *Bull. Amer. Meteor. Soc.*, **88**, 1589–1607.
- , K. Bedka, S. Paech, and L. Litten, 2008: A statistical evaluation of GOES cloud-top properties for nowcasting convective initiation. *Mon. Wea. Rev.*, **136**, 4899–4914.
- , W. M. Mackenzie, M. Koenig, and S. Muller, 2010: Cloud-top properties of growing cumulus prior to convective initiation as measured by Meteosat Second Generation. Part II. Use of visible reflectance. *J. Appl. Meteor. Climatol.*, **49**, 2544–2558.
- Merenti-Välimäki, H., and P. Laininen, 2002: Analysing effects of meteorological variables on weather codes by logistic regression. *Meteor. Appl.*, **9**, 191–197.
- Mosher, F., 2002: Detection of deep convection around the globe. Preprints, *10th Conf. on Aviation, Range, and Aerospace Meteorology*, Portland, OR, Amer. Meteor. Soc., 289–292.
- Nakajima, T., and M. King, 1990: Determination of the optical thickness and effective particle radius of clouds from reflected solar radiation measurements. Part I: Theory. *J. Atmos. Sci.*, **47**, 1878–1893.
- Negri, A., R. Adler, and P. Wetzel, 1984: Rain estimation from satellites: An examination of the Griffith–Woodley technique. *J. Climate Appl. Meteor.*, **23**, 102–116.
- Roberts, R., and S. Rutledge, 2003: Nowcasting storm initiation and growth using GOES-8 and WSR-88D data. *Wea. Forecasting*, **18**, 562–584.
- Roebeling, R., A. Feijt, and P. Stammes, 2006: Cloud property retrievals for climate monitoring: Implications of differences between Spinning Enhanced Visible and Infrared Imager (SEVIRI) on Meteosat-8 and Advanced Very High Resolution Radiometer (AVHRR) on NOAA-17. *J. Geophys. Res.*, **111**, D20210, doi:10.1029/2005JD006990.
- Rosenfeld, D., and G. Gutman, 1994: Retrieving microphysical properties near the tops of potential rain clouds by multi-spectral analysis of AVHRR data. *Atmos. Res.*, **34**, 259–283.
- , W. Woodley, A. Lerner, G. Kelman, and D. Lindsey, 2008: Satellite detection of severe convective storms by their retrieved vertical profiles of cloud particle effective radius and thermodynamic phase. *J. Geophys. Res.*, **113**, D04208, doi:10.1029/2007JD008600.
- Schmeits, M., K. Kok, D. Vogelesang, and R. van Westrhenen, 2008: Probabilistic forecasts of (severe) thunderstorms for the purpose of issuing a weather alarm in the Netherlands. *Wea. Forecasting*, **23**, 1253–1267.
- Schmetz, J., S. Tjemkes, M. Gube, and L. Van de Berg, 1997: Monitoring deep convection and convective overshooting with Meteosat. *Adv. Space Res.*, **19**, 433–441.

- , P. Pili, S. Tjemkes, D. Just, J. Kerkmann, S. Rota, and A. Ratier, 2002: An introduction to Meteosat Second Generation (MSG). *Bull. Amer. Meteor. Soc.*, **83**, 977–992.
- Setvák, M., and C. A. Doswell, 1991: The AVHRR channel 3 cloud top reflectivity of convective storms. *Mon. Wea. Rev.*, **119**, 841–847.
- Stammes, P., 2001: Spectral radiance modelling in the UV-visible range. *Current Problems in Atmospheric Radiation: Proceedings of the International Radiation Symposium*, W. L. Smith and Y. M. Timofeyev, Eds., A. Deepak, 385–388.
- Tag, P., R. Bankert, and L. Brody, 2000: An AVHRR multiple cloud-type classification package. *J. Appl. Meteor.*, **39**, 125–134.
- Thies, B., T. Nauß, and J. Bendix, 2008: Precipitation process and rainfall intensity differentiation using Meteosat Second Generation Spinning Enhanced Visible and Infrared Imager data. *J. Geophys. Res.*, **113**, D23206, doi:10.1029/2008JD010464.
- Tjemkes, S., L. Van de Berg, and J. Schmetz, 1997: Warm water vapour pixels over high clouds as observed by Meteosat. *Contrib. Atmos. Phys.*, **70**, 15–21.
- Wauben, W., H. K. Baltink, M. de Haij, N. Maat, and H. The, 2006: Status, evaluation and new developments of the automated cloud observations in the Netherlands. *TECO-2006—WMO Tech. Conf. on Meteorological and Environmental Instruments and Methods of Observation*, Geneva, Switzerland, World Meteorological Organization, 10 pp. [Available online at [http://www.wmo.int/pages/prog/www/IMOP/publications/IOM-94-TECO2006/1\(7\)\\_Wauben\\_Netherlands.pdf](http://www.wmo.int/pages/prog/www/IMOP/publications/IOM-94-TECO2006/1(7)_Wauben_Netherlands.pdf).]
- Wilks, D. S., 2006: *Statistical Methods in the Atmospheric Sciences*. 2nd ed. Academic Press, 627 pp.
- Zinner, T., H. Mannstein, and A. Tafferner, 2008: Cb-TRAM: Tracking and monitoring severe convection from onset over rapid development to mature phase using multi-channel *Meteosat-8* SEVIRI data. *Meteor. Atmos. Phys.*, **101**, 191–210.